Science of the Total Environment 572 (2016) 442–449

Contents lists available at ScienceDirect

Science of the Total Environment

journal homepage: www.elsevier.com/locate/scitotenv

A geostatistical approach to identify and mitigate agricultural nitrous oxide emission hotspots

P.A. Turner [a,*], T.J. Griffis [a], D.J. Mulla [a], J.M. Baker [a,b], R.T. Venterea [a,b]

[a] Department of Soil, Water, and Climate, University of Minnesota, 439 Borlaug Hall, 1991 Upper Buford Circle, St. Paul, MN 55108, USA
[b] United States Department of Agriculture – Agricultural Research Service, Soil and Water Management Unit, 1991 Upper Buford Circle, St. Paul, MN 55108, USA

HIGHLIGHTS

- Geospatial analyses resolved N_2O emissions at fine spatial scales.
- Hotspots emitted N_2O at rates >2-fold greater than non-hotspot locations.
- Targeted management of N_2O hotspots could reduce emissions by 17%.

GRAPHICAL ABSTRACT

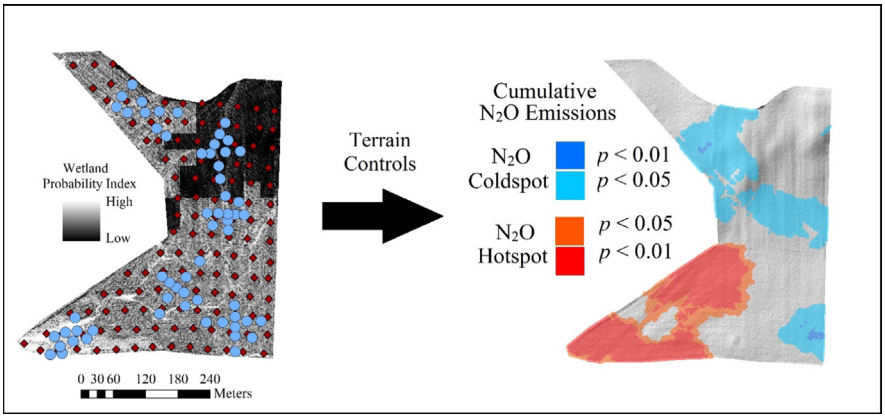

ARTICLE INFO

Article history:
Received 6 July 2016
Received in revised form 11 August 2016
Accepted 13 August 2016
Available online xxxx

Editor: Jay Gan

Keywords:
Nitrous oxide
Greenhouse gas management
Biogeochemical hotspots
LiDAR digital elevation model
Geospatial cokriging

ABSTRACT

Anthropogenic emissions of nitrous oxide (N_2O), a trace gas with severe environmental costs, are greatest from agricultural soils amended with nitrogen (N) fertilizer. However, accurate N_2O emission estimates at fine spatial scales are made difficult by their high variability, which represents a critical challenge for the management of N_2O emissions. Here, static chamber measurements ($n = 60$) and soil samples ($n = 129$) were collected at approximately weekly intervals ($n = 6$) for 42-d immediately following the application of N in a southern Minnesota cornfield (15.6-ha), typical of the systems prevalent throughout the U.S. Corn Belt. These data were integrated into a geostatistical model that resolved N_2O emissions at a high spatial resolution (1-m). Field-scale N_2O emissions exhibited a high degree of spatial variability, and were partitioned into three classes of emission strength: hotspots, intermediate, and coldspots. Rates of emission from hotspots were 2-fold greater than non-hotspot locations. Consequently, 36% of the field-scale emissions could be attributed to hotspots, despite representing only 21% of the total field area. Variations in elevation caused hotspots to develop in predictable locations, which were prone to nutrient and moisture accumulation caused by terrain focusing. Because these features are relatively static, our data and analyses indicate that targeted management of hotspots could efficiently reduce field-scale emissions by as much 17%, a significant benefit considering the deleterious effects of atmospheric N_2O.

© 2016 Elsevier B.V. All rights reserved.

Abbreviations: CV, coefficient of variation; DEM, digital elevation model; LiDAR, light detection and ranging; OC, ordinary cokriging; VNRA, variable rate nitrogen application; WPI, wetland probability index.

* Corresponding author.
E-mail address: turne289@umn.edu (P.A. Turner).

http://dx.doi.org/10.1016/j.scitotenv.2016.08.094
0048-9697/© 2016 Elsevier B.V. All rights reserved.

1. Introduction

Nitrous oxide (N_2O) is a potent greenhouse gas (Hartmann et al., 2013) and the leading cause of stratospheric ozone loss (Ravishankara et al., 2009). In response to its deleterious environmental effects, efforts to mitigate agricultural emissions, which account for nearly 75% of the national anthropogenic source (US Department of State, 2014), are in development. Such efforts often focus on N management improvements (e.g., optimizing the source, depth, and timing of fertilizer) at the field or farm scale. Yet, the findings from these mitigation strategies have been highly variable (Venterea et al., 2016), in part because episodic and spatially variable emissions hinder accurate budget estimates (Mathieu et al., 2006; Velthof et al., 2000). For instance, field-scale N_2O emission measurements with chambers can yield a coefficient of variation (CV) as high as 500% (Folorunso and Rolston, 1984; van den Pol-van Dasselaar et al., 1998), suggesting that our ability to accurately determine the outcome of mitigation practices is cause for concern. At fine sub-field spatial scales (<1 m^2 to 1000 m^2), N_2O "hotspots" appear to be disproportionately strong sources (Parkin, 1987; van den Heuvel et al., 2009), yet their influence over cumulative field-scale emissions remains uncertain because high-resolution data are rarely available. For farmers to manage N_2O emissions effectively, subfield-scale emission estimates are necessary to identify potential hotspots and to benchmark their effects on field-scale mitigation practices.

Light detection and ranging (LiDAR) digital elevation models (DEMs) are powerful tools that can help guide precision agriculture and conservation strategies (Galzki et al., 2011; Wan et al., 2014). When coupled with geospatial techniques, this emerging technology helps generate high-resolution maps of agriculturally relevant information such as the presence of hydric soils (Fink and Drohan, 2016), moisture content (Moore et al., 1993; Murphy et al., 2009), and soil nitrogen status (Weintraub et al., 2014) that allow farmers to focus extra attention and resources on critical areas. Furthermore, complex processes like methane emissions (Sundqvist et al., 2015) have been characterized using DEMs, suggesting that this technology can better resolve the field-scale spatial distribution of N_2O emissions.

Indeed, differences in topography and landscape position have a strong influence on N_2O emissions (Ambus, 1998; Ball et al., 1997) because terrain gradients redistribute moisture and nutrients that are necessary for the production of N_2O. Consequently, N_2O emission frequency distributions are typically positively skewed by a few strong sources (Parkin, 1987; Velthof et al., 2000) observed at topographically low positions (Ambus, 1998). Here, terrain focusing enables the development of hotspots by concentrating organic matter, moisture, and nitrate (NO_3^-) into localized, but potentially predictable areas. Taken together, these soil characteristics can support disproportionately high rates of denitrification (Groffman et al., 2009) that we posit are capable of sustaining high N_2O emissions. However, field-scale emission distribution maps remain coarse, since an unrealistic number of static chambers are required to resolve the high variability, implying poor constraints on hotspots.

With the aid of DEMs and geospatial analyses, denitrification hotspots can be isolated and mapped by pinpointing locations with the highest probability of moisture and NO_3^- accumulation (Anderson et al., 2015). We propose that a similar approach can resolve the distribution of N_2O emissions at a high spatial resolution that will guide targeted mitigation practices. Here, we examine the spatial distribution of N_2O fluxes and cumulative emissions in a strip-tilled cornfield to address three questions: 1) can DEMs help predict where N_2O hotspots will develop on the landscape; 2) how significant are hotspots in the cumulative field-scale budget; and 3) how can DEMs be used to guide N management and N_2O mitigation?

2. Materials and methods

2.1. Site description and experimental design

The tile-drained, corn-soybean rotation research field (15.6-ha) was located on a private farm 11-km south of Northfield, Minnesota (44°21′37.2″N, 93°12′14.8″W). The predominant underlying soil is a Prinsburg silty clay loam (Typic Endoaquolls, USDA Classification) overlying a loam. Measurements were made during the corn (*Zea mays*, L.) phase in 2014 on DOY 126, 134, 150, 156, 161, and 168. The field was strip-tilled prior to planting and fertilized with 32% urea ammonium sulfate (UAS) on DOY 125 at a rate of 140 kg N ha^{-1}.

A 3-m micrometeorological tower was installed on the west side of the field to measure air temperature (VP-4; Decagon Devices, Pullman, WA, USA). Observations were recorded with a data logger at 5-min intervals and averaged hourly (Model EM50; Decagon Devices, Pullman, WA, USA).

All soil and chamber sample locations were georeferenced using a GPS device (GeoXH; Trimble, Sunnyvale, CA, USA) connected to a Mi-Fi mobile hotspot (model 2200; Verizon Wireless, Wallingford, CT, USA) that boosted the horizontal accuracy to 0.1 m. Spatial data were analyzed using ArcMap (ArcGIS v.10.2; ESRI Inc., Redlands, CA, USA).

To capture the effects of terrain on N_2O emissions and to ensure potential hotspots were included in the measurement campaign, a Wetland Probability Index (WPI) map was created (ArcGIS v.10.2; ESRI Inc., Redlands, CA, USA) to guide the experimental design. The WPI is a regression function of four factors: the presence of hydric soils, slope, profile curvature, and a compound topographic index (CTI) that is a function of flow accumulation and slope. The WPI provides a relative metric to describe the likelihood that water will pond at a specific location and has been used to identify areas for efficient wetland reclamation (Wan et al., 2014). The WPI was chosen rather than the widely used soil wetness index (SWI), because the WPI incorporates drainage (hydric soils), a recognized shortcoming of the idealized SWI (Murphy et al., 2009). In the context of N_2O production, field locations with wetland terrain characteristics are likely to accumulate moisture and nutrients and are thus candidates for hotspot formation. These areas are likely to experience more frequent and prolonged periods of soil saturation than upland areas, in part because of low slopes and elevation. Using high-resolution (1-m) DEM data (Minnesota Geospatial Information Office) and soil survey information, each position on the landscape was assigned a relative WPI value of 0 to 1 (Wan et al., 2014).

Since the natural movement of soil moisture is not confined to the explicit 1-m WPI grid, the highest spatial resolution is not necessarily appropriate for direct comparison with a dependent variable (Sørensen and Seibert, 2007). For instance, contour cropping, crop residues, buffer strips and microtopography can affect the movement of moisture. To minimize these uncertainties, we have reduced the WPI resolution to 10-m (Anderson et al., 2015; Zhang and Montgomery, 1994) for direct comparison of N_2O emission measurements and surface characteristics. All other analyses used the high-resolution WPI data set.

Because terrain differences can influence emissions, a stratified sampling design based on WPI was used to characterize emission heterogeneity. Groups ($n = 6$) of chambers ($n = 10$) were installed in the field across a range of WPI values on each of the sample dates. Measurements were taken at approximately weekly intervals for 42-d immediately after fertilization (DOY 125). Previous experiments in this field indicate that N_2O fluxes are highest in the 20 to 50-d following fertilization (Baker et al., 2014; Fassbinder et al., 2013). Beyond this time frame, N_2O fluxes decline (Baker et al., 2014; Turner et al., 2016a) and as a result, the cumulative emission budget is most sensitive to loss during this brief period.

2.2. Nitrous oxide measurements

Soil N_2O fluxes were measured manually with non-flow-through non-steady-state chambers with a design that has been used extensively in agricultural systems (Maharjan and Venterea, 2014; Maharjan et al., 2014; Venterea and Coulter, 2015). Briefly, each chamber consisted of a stainless steel base inserted 0.05-m into the soil and a removable top (0.50 m × 0.29 m × 0.086 m). Weather stripping and spring clamps attached to opposing sides sealed the chamber headspace from ambient mixing. Each chamber top was vented and covered with an insulated, reflective material. Measurements were taken after at least 48-h following chamber installation to avoid the potential influence of soil disturbance on the flux.

Gas samples were taken from between 0900 and 1500 local time at 0, 15, 30, and 45 min intervals using a 12-mL polypropylene syringe inserted through a butyl rubber septum on the chamber lid. An ambient air sample was taken immediately after chamber closure. Samples were immediately transferred into glass vials sealed with butyl rubber septa and analyzed within one week using a headspace autosampler (Teledyne Tekmar; Mason, OH, USA) connected to a gas chromatograph (model 5990; Agilent/Hewlett-Packard, Santa Clara, CA, USA) equipped with an electron capture detector. Helium was used as the carrier gas in the GC analyses and the system was calibrated with analytical standards (Scott Specialty Gases, MI) (Bavin et al., 2009). Concentrations from the GC were converted into mass per volume units, assuming ideal gas relations and a known air temperature while sampling.

The slope of the chamber headspace gas concentration was determined using either a linear regression or a quadratic model depending on the curvilinearity of the slope (Parkin et al., 2012; Venterea, 2013). The linear slope was calculated using the SLOPE function (Excel v.2013; Microsoft, Redmond, WA) and the quadratic slope was estimated using the LINEST function at time zero. The quadratic model accounts for suppression of the concentration gradient in response to chamber closure, but is not always necessary. A linear slope was chosen if the second derivative of the quadratic equation was greater than zero (Maharjan et al., 2014). Soil fluxes were calculated using:

$$F = \frac{S * V}{A} \quad (1)$$

where: S is the slope, V is the chamber volume (0.02-m^3), and A (0.14-m^2) is the chamber footprint. Cumulative N_2O emissions were calculated using trapezoidal integration that assumes linearity between sampling periods.

2.3. Soil analyses

Within 24-hours of gas sampling, soil samples ($n = 129$) to a depth of 0.15-m were taken from a georeferenced 35-m grid using a hand corer. Soil samples were weighed within 2 h. After drying at 105 °C, gravimetric water content (θ) was determined. Using a 2 M KCl extraction, soil NO_3^- concentration was also determined (Maharjan and Venterea, 2014). Extracts were filtered (Whatman no. 1) and NO_3^- was quantified using a flow-through injection analyzer (Lachat, Loveland, CO, USA). The NO_3^- intensity ($NO_3^-{}_{int}$) was calculated using trapezoidal integration (Maharjan and Venterea, 2014; Venterea et al., 2011), which assumes a linear slope between sample dates. Conceptually, $NO_3^-{}_{int}$ represents the cumulative exposure of soil microbes to NO_3^-. The θ intensity (θ_{int}) was calculated similarly. Stepwise regression models were used to identify any terrain indices that were significantly correlated with soil chemical variables.

2.4. Geostatistical analyses

Interpolations of high-resolution N_2O flux and cumulative emission data were performed with ordinary cokriging (OC) in ArcMap (ArcGIS v.10.2; ESRI Inc., Redlands, CA, USA). Ordinary cokriging is a geostatistical approach that uses more frequently sampled secondary variables to improve prediction of the primary variable (Vauclin et al., 1983). This method is useful when the primary attribute is costly or logistically more difficult to sample than other correlated variables.

Mean N_2O fluxes and cumulative emissions were interpolated at a resolution of 1-m with OC using an omnidirectional "stable" model. Soil NO_3^- and θ were used as secondary variables in this OC model. The sill (variance), nugget (estimate of independent or micro-scale errors), and range (maximum distance of autocorrelation) of each model were estimated from the semivariogram. The model parameters were optimized for estimation of the range value and neighborhood weights were based on distance. Cross validation was accomplished iteratively by comparing the observation to the OC model predicted value. All inputs were log transformed prior to OC to meet the assumption of normality.

A Getis-Ord Gi* statistical test identified spatial clustering of high (hotspots) and low (coldspots) emissions at a 95% significance threshold (Ord and Getis, 2010). The field was partitioned into three emission classes based on their respective z-score significance using ArcMap (ArcGIS v.10.2; ESRI Inc., Redlands, CA, USA). Locations with statistically significant high and low z-scores are referred to as emission hotspots and coldspots, respectively. All other values, i.e. those with insignificant ($p > 0.05$) z-scores, are considered "intermediate" locations. A Kruskal-Wallis significance test ($\alpha = 0.05$) was used to determine if there was a WPI difference among emission classes.

3. Results and discussion

3.1. Meteorology and soil characteristics

Over the course of our measurement campaign, this field received 116.8 mm of precipitation and experienced a mean air temperature of 16.4 °C. Across all sampling dates, the mean (range) soil NO_3^- concentration and θ content were 20.5 (0–107) mg NO_3^- kg^{-1} and 25% (12–50), respectively (Fig. 1). Reported NO_3^- concentration and θ content frequency distributions were positively skewed on each sample date (data not shown), indicating the potential for nutrient processing hotspots. Following fertilization on DOY 125, the daily mean soil NO_3^- concentrations increased until DOY 157, after which they started declining, likely as a result of a combination of leaching, denitrification, and crop uptake.

Analyses indicated that the WPI (10-m) was significantly ($p < 0.05$) correlated with θ_{int} and $NO_3^-{}_{int}$ observations ($r^2 = 0.6$ and $r^2 = 0.14$, respectively) (Fig. 2). These relationships provide evidence of terrain focusing, implicit in the WPI calculation (e.g., elevation, slope). Indeed, measurements of θ_{int} were significantly ($p < 0.05$) and negatively correlated with both elevation ($r^2 = 0.6$) and slope ($r^2 = 0.4$). Observations of $NO_3^-{}_{int}$ were not as tightly coupled to elevation ($r^2 = 0.09$) or slope ($r^2 = 0.05$) as θ_{int}, probably because of the complex N cycling dynamics (i.e. including both production and consumption of NO_3^-) present in soils. Overall, the samples with the highest θ_{int} and $NO_3^-{}_{int}$ were observed in locations with the lowest slope and elevation (Fig. 2), suggesting that the soil factors necessary to sustain high denitrification fluxes can become concentrated in predictable areas. This finding provides further support that remote sensing techniques can offer important insights into field-scale N processing dynamics by identifying locations that have an elevated likelihood of moisture and nutrient accumulation (Anderson et al., 2015; Weintraub et al., 2014).

3.2. N_2O emissions

3.2.1. Temporal dynamics

Across all chambers and sampling dates, the mean (range) N_2O flux was 1.7 (−1 − 32) mg N_2O—N m^{-2} d^{-1}. The magnitude of N_2O fluxes ranged from 0.7 mg N_2O—N m^{-2} d^{-1} on DOY 126, within 24-h of

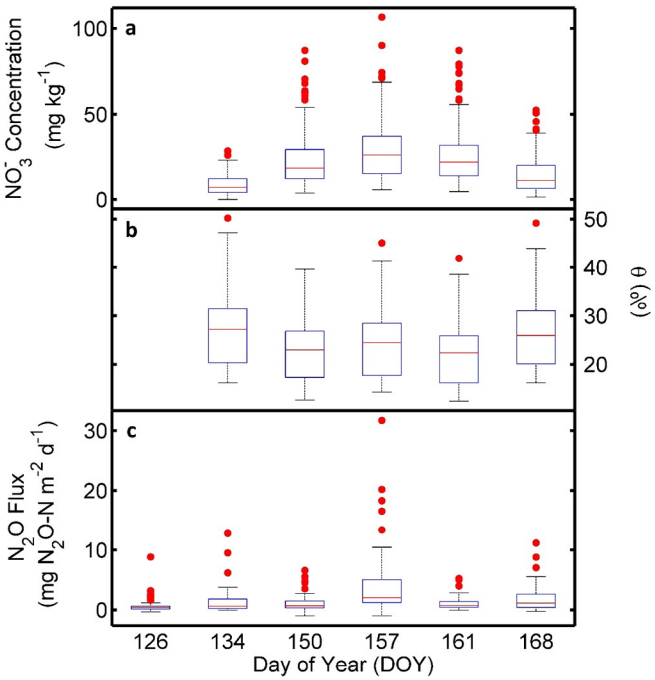

Fig. 1. Boxplots of a) NO_3^- concentration (mg NO_3^- kg^{-1}), b) gravimetric moisture content (%), and c) N_2O flux density (mg N_2O—N m^{-2} d^{-1}). Red points designate outliers.

fertilization, to a peak emission of 4.3 mg N_2O—N m^{-2} d^{-1} on DOY 157, and decreased to a value of 1.8 mg N_2O—N m^{-2} d^{-1} on DOY 168 (Fig. 1). Over the sample period, the average N_2O flux was positively correlated ($r^2 = 0.06$; $p < 0.05$) to WPI (10-m), indicative of a terrain signal. Indeed, elevation ($r^2 = 0.12$; $p < 0.01$) and slope ($r^2 = 0.04$; $p = 0.06$) correlated with average N_2O fluxes (Fig. 3).

These hourly mean flux density observations are comparable in strength to a previous study that used 6 automated chambers to estimate the annual N_2O budget at this field site during the 2010 corn phase (Fassbinder et al., 2013). Those investigators determined that N_2O emissions were elevated for 20 to 50 days after fertilization, but then losses declined precipitously and the average hourly standard deviation fell 14-fold, suggesting relatively low temporal measurement uncertainty beyond this brief period (Fassbinder et al., 2013).

3.2.2. Spatial dynamics

Trapezoidal integration of chamber data indicated that the mean (SD) cumulative N_2O emission was 69 (61) mg N_2O—N m^{-2} during the 42-d sampling period. We calculated a field-scale CV of 88% from the cumulative chamber data, which is lower than some investigations (Ambus and Christensen, 1995; Ball et al., 1997; Folorunso and Rolston, 1984; Jones et al., 2011; Molodovskaya et al., 2011) and significantly higher than others (Christensen et al., 1996). The reason for our comparatively low CV may have been because our sample size ($n = 60$) was relatively large compared to those previous studies and better captured the spatial heterogeneity. Contrary to our hypothesis, there was not a significant relationship ($r^2 = 0.03$; $p = 0.1$), between the WPI (10-m) and cumulative N_2O emissions (Fig. 3). The low r^2 was probably the result of other factors that influence emissions but were not explicitly included in our model, e.g., pH, gas diffusivity, and sources of N_2O other than denitrification including nitrification (Kool et al., 2011; Venterea et al., 2015). Similarly, slope ($r^2 = 0.04$; $p = 0.08$) was not a significant correlate with N_2O emissions either (Fig. 3). However, elevation ($r^2 = 0.09$; $p < 0.05$) exhibited a negative, although weak relation to N_2O emissions (Fig. 3), indicating that topographic position can affect N_2O production.

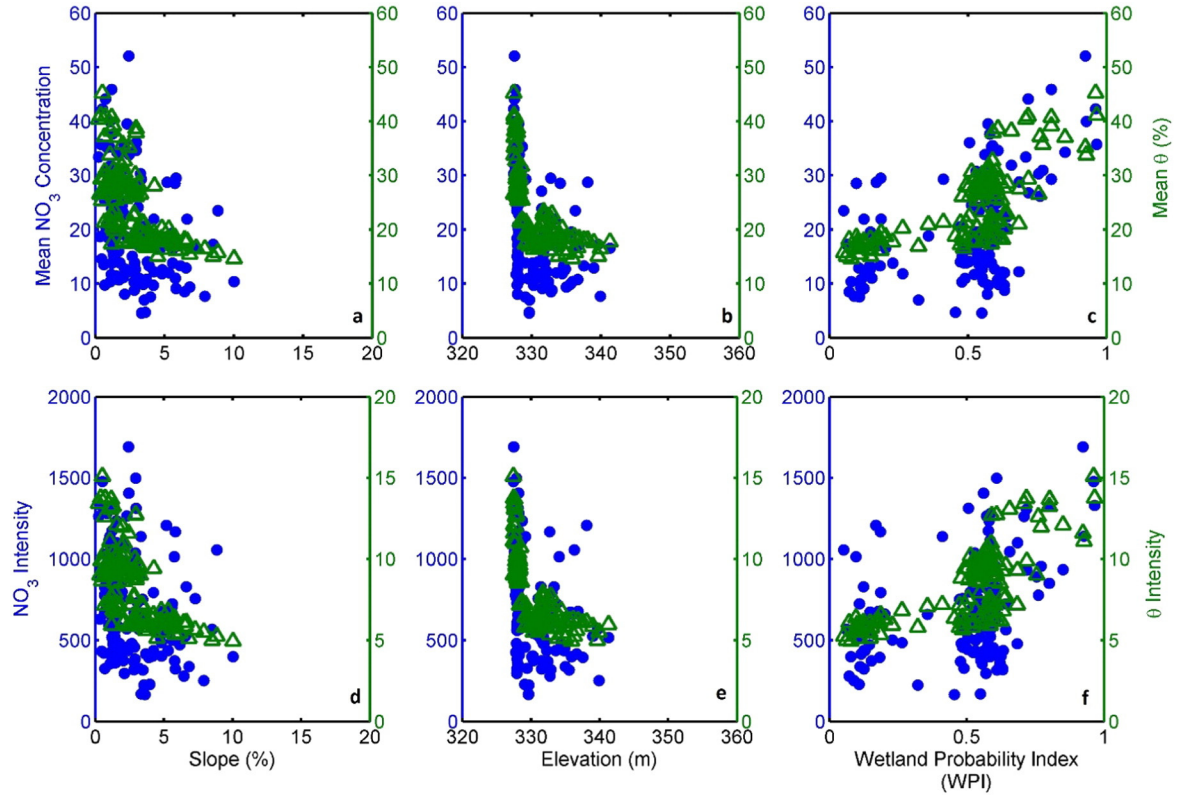

Fig. 2. Plotted relationships between topographic indices and soil characteristics ($n = 129$). Top row). Mean soil NO_3^- concentration (blue dots); mean gravimetric water content (θ; green triangles). Bottom row). Integrated soil NO_3^- ($NO_3^-{}_{int}$; blue dots); integrated gravimetric water content (θ_{int}; green triangles). (For interpretation of the references to color in this figure legend, the reader is referred to the web version of this article.)

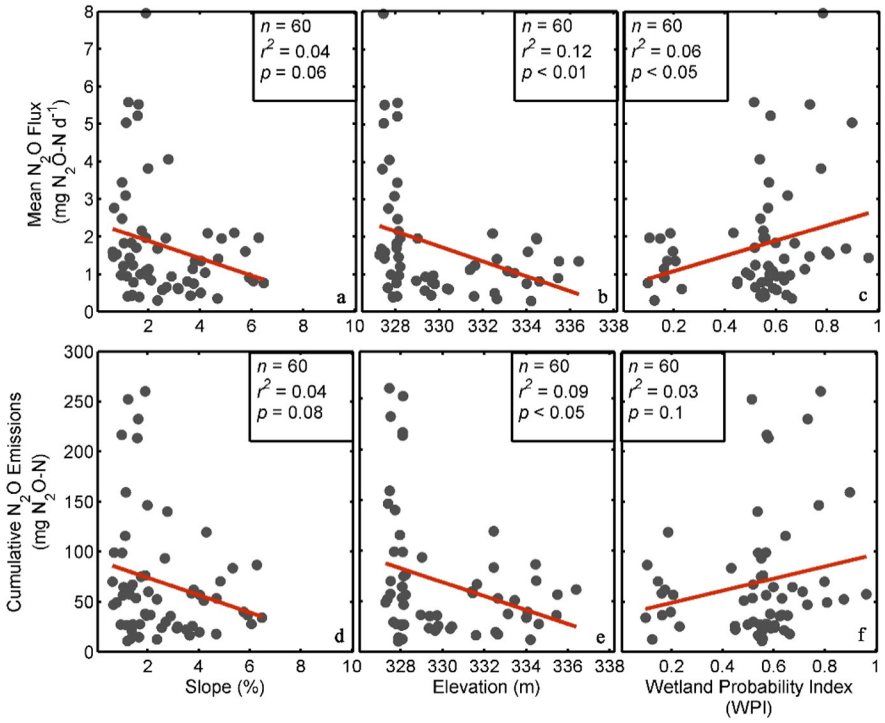

Fig. 3. Plotted relationships between mean N_2O fluxes (a, b, and c) and cumulative N_2O emissions (d, e, and f) over the measurement period against topographic indices ($n = 60$). Lines of linear best fit (red lines) for each graph are included. (For interpretation of the references to color in this figure legend, the reader is referred to the web version of this article.)

Based on a priori hypotheses, θ_{int} and $NO_3^-{}_{int}$ were included as secondary OC variables to improve the average N_2O flux and cumulative emission model prediction ($n = 156{,}190$). Cross-validation of cumulative emissions determined that an omnidirectional stable model was appropriate. Stable model semivariograms indicate that the sill, nugget, and range of the average N_2O flux were 0.59 mg N_2O—N m^{-2} d^{-2}, 0.37 mg N_2O—N m^{-2} d^{-2}, and 244-m, respectively, while the sill, nugget, and range of the cumulative emissions were 0.7 mg N_2O—N^2 m^{-2}, 0.43 mg N_2O—N^2 m^{-2}, and 320-m, respectively (data not shown). As a measure of variance, the sill provides a field-scale estimate of spatial uncertainty, while the nugget is an estimate of either measurement uncertainty or microscale variation (Yanai et al., 2003). Here, a large nugget effect suggests large uncertainty at fine-scales. Observations taken from points separated by a distance greater than the range are no longer spatially autocorrelated, a point identified in the semivariogram where variance becomes asymptotic (i.e. the sill).

During the measurement period, the field emitted on average (SD) 1.4 (0.6) mg N_2O—N m^{-2} d^{-1}, with a 43% CV, more than half that of the original chamber data (Fig. 4). Cumulatively, the OC model predicted that 8.7 kg N_2O—N were emitted over the 42-d measurement (Fig. 3). This translates to a field-scale mean (SD) cumulative flux of 55.4 (22) mg N_2O—N m^{-2}. The emission distribution was positively skewed, indicating that the data set was likely affected by hotspots. Because soil samples were not taken at each individual chamber, OC interpolations of $NO_3^-{}_{int}$ and θ_{int} at each chamber were extracted to assess their relationships with cumulative N_2O emissions. These data show that

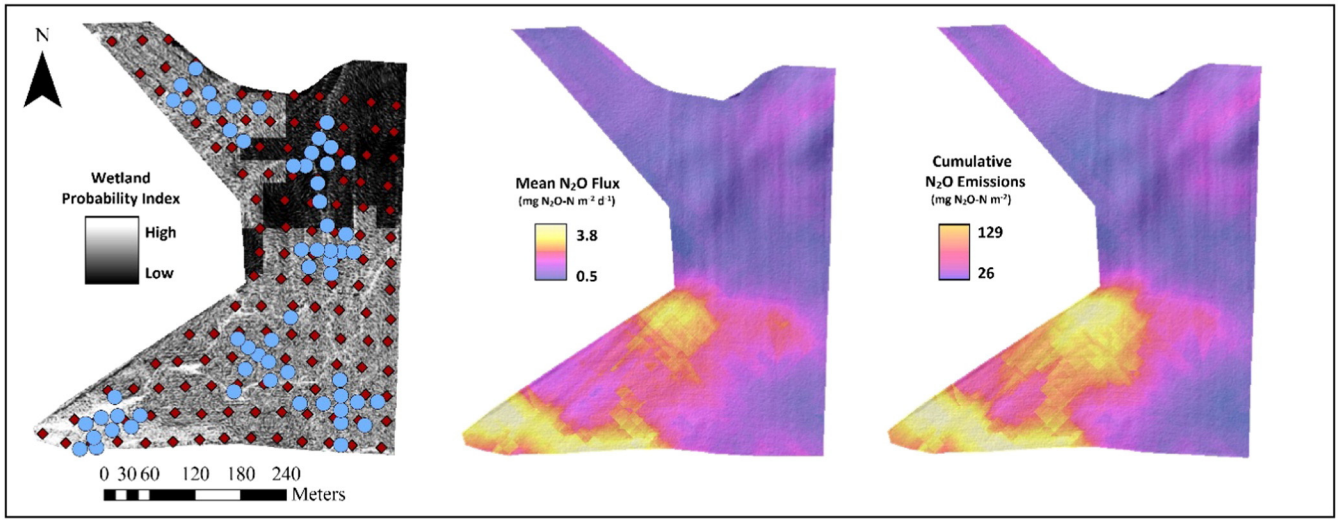

Fig. 4. The Wetland Probability Index (WPI) overlain with chamber measurements (blue circles) and soil samples (red diamonds). Results are presented from the N_2O ordinary cokriging model, which interpolated mean flux density and cumulative emissions at a 1-m spatial resolution. (For interpretation of the references to color in this figure legend, the reader is referred to the web version of this article.)

cumulative N_2O emissions were significantly ($p < 0.01$) correlated with $NO_3^-{}_{int}$ ($r^2 = 0.25$) and θ_{int} ($r^2 = 0.18$) predictions (Fig. 5).

Using a Getis Ord Gi* statistical analysis, locations in this field were partitioned into three classes based on their emission strength within the context of neighboring values (Ord and Getis, 2010). These analyses identified significant clustering of high and low N_2O emissions, characteristic of hotspots and coldspots, respectively (Fig. 6). The mean (SD) flux from hotspots, intermediate, and coldspot locations was 2.5 (0.4) mg N_2O—N m^{-2} d^{-1}, 1.3 (0.3) mg N_2O—N m^{-2} d^{-1}, and 0.8 (0.05) mg N_2O—N m^{-2} d^{-1}, respectively. Cumulatively, 3.1 kg N_2O—N, 4.6 kg N_2O—N, and 0.9 kg N_2O—N were emitted from hotspots, intermediate, and coldspot locations, respectively.

These analyses indicate that a disproportionate share of the field-scale emission budget can be attributed to hotspot locations. Here, hotspots were responsible for 36% of the cumulative N_2O emission budget despite occupying only 21% of the field, while coldspots emitted 11% of the cumulative budget from a comparable area (18%). The remaining N_2O emissions (53%) were lost from intermediate locations, largely because 61% of the land surface fell under this emission class. However, the area of a field that qualifies as a hotspot could fluctuate based on meteorology — for instance, a particularly wet spring could increase the surface area of locations that experience prolonged and high moisture exposure. Kruskal-Wallis tests showed that the WPI observed in hotspot locations was greater than the WPI values typically found in the other emission classes, in part because these locations had low slopes and elevation. A Kruskal-Wallis test revealed that hotspots had statistically different slopes (mean = 1.6%) and elevation (mean = 327.8-m) than intermediate (mean = 3.3%; 331.4-m) or coldspot (mean = 3.7%; 331.1-m) locations (data not shown).

Consequently, the general locations of hotspots were largely static, likely because of the strong relation with topographic indices, including elevation and slope. The positive relations identified here indicate that topography, via its controls on nutrient and moisture distributions, can help guide N_2O management practices. Towards this end, the disproportionate strength and stability of N_2O hotspots indicates that targeted management of these sources could efficiently reduce total emissions. For instance, if the average hotspot flux density were reduced from 2.5 mg N_2O—N m^{-2} d^{-1} to 1.3 (0.3) mg N_2O—N m^{-2} d^{-1}, 1, a magnitude that is more in step with intermediate areas, the mean field-scale flux density over the entire measurement period could be reduced by up to 14% (10–18). By reducing the cumulative hotspot emissions to 49 (10.4) mg N_2O—N m^{-2}, the rate observed in intermediate areas, the field-scale budget could be reduced by as much as 17% (12 − 22). The removal of hotspots through native wetland reclamation could reduce emissions by as much as 36%. Given the strong radiative forcing and other side effects of N_2O, these findings deserve serious consideration, especially if the distribution of potential hotspots is similarly predictable throughout the U.S. Corn Belt.

From a management perspective, emission hotspots were generally collocated with $NO_3^-{}_{int}$ hotspots. Consequently, variable rate nitrogen application (VRNA), a recent advancement in precision agriculture, could prove an effective tool to address N_2O hotspots. This technology translates crop reflectance readings into fine-scale fertilizer decisions and has been shown to increase yield and income while providing promising N uptake results (Scharf et al., 2011). Better soil N management overall will potentially reduce N_2O emissions; however, the one-size-fits-all approach to fertilizer application may be a contributing factor to hotspots that VRNA can overcome. For instance, because low-lying areas accumulate surplus NO_3^- from upland areas and may not require additional N, VRNA can limit over application. Further, easing the NO_3^- surplus in upland areas using fine-scale fertilizer decisions could help mitigate the effects of terrain focusing. Alternatively, the selective application of enhanced efficiency N fertilizers (EENFs), which show promising N_2O mitigation results (Halvorson et al., 2014), to hotspots via VRNA could minimize their strength. However, extrapolating the effect EENFs may have on hotspots here becomes difficult since EENF results are often specific to soil type and climate.

These data also showed that N_2O and θ_{int} hotspots were collocated, suggesting that N_2O hotspots are most likely to require subsurface drainage to ensure crop success. If conservation wetlands or VRNA were capable of reducing NO_3^- losses in tile drainage, either by improving N uptake for target and non-target species (i.e., wetland plants) or by reduced subsurface drainage overall, indirect emissions downstream could also be mitigated (Turner et al., 2016b). A reduction of offsite nitrate losses, like those from leaching and runoff, would be an important benefit because these can be disproportionately strong sources of N_2O, especially in the Corn Belt (Chen et al., 2016; Griffis et al., 2013; Turner et al., 2015). However, little is known about emissions from conservation wetlands or the ultimate N_2O effect from VRNA.

Since our data set only includes six sample dates, these analyses may not include episodic emissions and therefore likely represent a conservative estimate. To resolve this uncertainty, automated soil chambers are an effective means for taking high frequency measurements (Baker et al., 2014; Turner et al., 2016a). However, sampling constraints (e.g., cost, tube length, and on-site power) tether chambers to a central point, limiting their ability to capture the spatial distribution of emissions observed here. Therefore, the potential for terrain artifacts to bias measurements must be considered when selecting chamber placement. For instance, past work in this field explored various N_2O treatment effects using an automated chamber system (Baker et al., 2014; Fassbinder et al., 2013). Although, those experiments were situated in a location that our analyses has classified as an intermediate strength

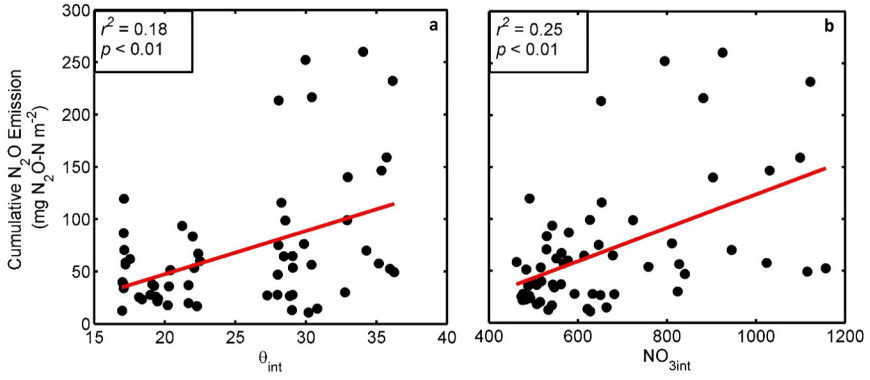

Fig. 5. The relationship between cumulative N_2O emissions and the soil characteristics, $NO_3^-{}_{int}$ and θ_{int}. A linear line of best fit is included (red). (For interpretation of the references to color in this figure legend, the reader is referred to the web version of this article.)

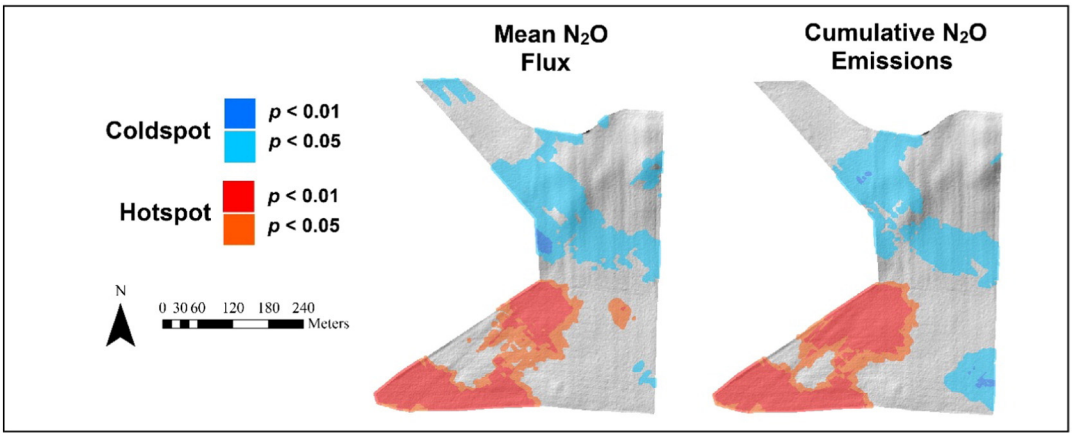

Fig. 6. Results from the Getis Ord Gi* statistic that was used to identify the spatial distribution of hotspots and coldspots. Intermediate locations are transparent.

emitter, they highlight the risks of automated chamber clusters in hotspot or coldspot regions.

4. Conclusion

Our data and analyses have shown that LiDAR DEMs and geospatial techniques can be valuable tools to resolve hotspots and model fine-scale N_2O emissions. Here, hotspots were disproportionately strong sources, responsible for more than a third of the cumulative emissions. Because hotspots are reliant on terrain focusing for nutrients and moisture, they are relatively static features. Consequently, their regularity and predictability should facilitate targeted management practices that could reduce field-scale emissions by as much as 17%.

(For interpretation of the references to color in this figure legend, the reader is referred to the web version of this article.)

Acknowledgements

We thank Jeff Wood, Matt Erickson, Mike Dolan, William Breiter, Ke Xiao, Zichong Chen, and Lucas Rosen for field and laboratory assistance. This work was supported by the U.S. Department of Agriculture (USDA) Grant USDA-NIFA 2013-67019-21364 and the USDA – Agricultural Research Service. We are also appreciative of the private landowner who volunteered their field for our use.

References

Ambus, P., 1998. Nitrous oxide production by denitrification and nitrification in temperate forest, grassland and agricultural soils. Eur. J. Soil Sci 49, 495–502.

Ambus, P., Christensen, S., 1995. Spatial and seasonal nitrous oxide and methane fluxes in Danish forest, grassland, and agroecosystems. Atmos. Pollut. Trace Gases 24, 993–1001.

Anderson, T.R., Groffman, P.M., Walter, M.T., 2015. Using a soil topographic index to distribute denitrification fluxes across a northeastern headwater catchment. J. Hydrol. 522, 123–134. http://dx.doi.org/10.1016/j.jhydrol.2014.12.043.

Baker, J.M., Fassbinder, J., Lamb, J.A., 2014. The impact of corn stover removal on N_2O emission and soil respiration: an investigation with automated chambers. Bioenergy Res. 7, 503–508. http://dx.doi.org/10.1007/s12155-014-9412-1.

Ball, B.C., Horgan, G.W., Clayton, H., Parker, J.P., 1997. Spatial variability of nitrous oxide fluxes and controlling soil and topographic properties. J. Environ. Qual. 26, 1399. http://dx.doi.org/10.2134/jeq1997.00472425002600050029x.

Bavin, T.K., Griffis, T.J., Baker, J.M., Venterea, R.T., 2009. Impact of reduced tillage and cover cropping on the greenhouse gas budget of a maize/soybean rotation ecosystem. Agric. Ecosyst. Environ. 134, 234–242. http://dx.doi.org/10.1016/j.agee.2009.07.005.

Chen, Z., Griffis, T.J., Millet, D.B., Wood, J.D., Lee, X., Baker, J.M., Xiao, K., Turner, P.A., Chen, M., Zobitz, J., Wells, K.C., 2016. Partitioning N_2O emissions within the US Corn Belt using an inverse modeling approach. Glob. Biogeochem. Cycles http://dx.doi.org/10.1002/2015GB005313.

Christensen, S., Ambus, P., Arah, J.R.M., Clayton, H., Galle, B., Griffith, D.W.T., Hargreaves, K.J., Klemedtsson, L., 1996. Nitrous oxide emission from an agricultural field: comparison between measurements by flux chamber and micrometerological techniques. Atmos. Environ. 30, 4183–4190. http://dx.doi.org/10.1016/1352-2310(96)00145-8.

Fassbinder, J.J., Schultz, N.M., Baker, J.M., Griffis, T.J., 2013. Automated, low-power chamber system for measuring nitrous oxide emissions. J. Environ. Qual. 42, 606–614. http://dx.doi.org/10.2134/jeq2012.0283.

Fink, C.M., Drohan, P.J., 2016. High resolution hydric soil mapping using LiDAR digital terrain modeling. Soil Sci. Soc. Am. J. 80, 355–363. http://dx.doi.org/10.2136/sssaj2015.07.0270.

Folorunso, O.A., Rolston, D.E., 1984. Spatial variability of field-measured denitrification gas fluxes. Soil Sci. Soc. Am. J. 48, 1214–1219. http://dx.doi.org/10.2136/sssaj1984.03615995004800060002x.

Galzki, J.C., Birr, A.S., Mulla, D.J., 2011. Identifying critical agricultural areas with three-meter LiDAR elevation data for precision conservation. J. Soil Water Conserv. 66, 423–430. http://dx.doi.org/10.2489/jswc.66.6.423.

Griffis, T.J., Lee, X., Baker, J.M., Russelle, M.P., Zhang, X., Venterea, R., Millet, D.B., 2013. Reconciling the differences between top-down and bottom-up estimates of nitrous oxide emissions for the U.S. Corn Belt. Glob. Biogeochem. Cycles 27, 746–754. http://dx.doi.org/10.1002/gbc.20066.

Groffman, P.M., Butterbach-Bahl, K., Fulweiler, R.W., Gold, A.J., Morse, J.L., Stander, E.K., Tague, C., Tonitto, C., Vidon, P., 2009. Challenges to incorporating spatially and temporally explicit phenomena (hotspots and hot moments) in denitrification models. Biogeochemistry 93, 49–77. http://dx.doi.org/10.1007/s10533-008-9277-5.

Halvorson, A.D., Snyder, C.S., Blaylock, A.D., Del Grosso, S.J., 2014. Enhanced-efficiency nitrogen fertilizers: potential role in nitrous oxide emission mitigation. Agron. J. 106, 715. http://dx.doi.org/10.2134/agronj2013.0081.

Hartmann, D.L., Klein Tank, A.M.G., Rusticucci, M., Alexander, L.V., Brönnimann, S., Charabi, Y.A.-R., Dentener, F.J., Dlugokencky, E.J., Easterling, D.R., Kaplan, A., Soden, B.J., Thorne, P.W., Wild, M., Zhai, P., 2013. Observations: atmosphere and surface. Climate Change 2013: The Physical Science BasisContribution of Working Group I to the Fifth Assessment Report of the Intergovernmental Panel on Climate Change. Cambridge University Press http://dx.doi.org/10.1017/CBO9781107415324.008.

Jones, S.K., Famulari, D., Di Marco, C.F., Nemitz, E., Skiba, U.M., Rees, R.M., Sutton, M.a., 2011. Nitrous oxide emissions from managed grassland: a comparison of eddy covariance and static chamber measurements. Atmos. Meas. Tech. 4, 2179–2194. http://dx.doi.org/10.5194/amt-4-2179-2011.

Kool, D.M., Dol, J., Wrage, N., Willem, J., Groenigen, V., 2011. Soil biology & biochemistry nitrifier denitrification as a distinct and significant source of nitrous oxide from soil. Soil Biol. Biochem. 43, 174–178. http://dx.doi.org/10.1016/j.soilbio.2010.09.030.

Maharjan, B., Venterea, R.T., 2014. Anhydrous ammonia injection depth does not affect nitrous oxide emissions in a silt loam over two growing seasons. J. Environ. Qual. 43, 1527–1535. http://dx.doi.org/10.2134/jeq2014.07.0292.

Maharjan, B., Venterea, R.T., Rosen, C., 2014. Fertilizer and irrigation management effects on nitrous oxide emissions and nitrate leaching. Agron. J. 106, 703–714. http://dx.doi.org/10.2134/agronj2013.0179.

Mathieu, O., Lévêque, J., Hénault, C., Milloux, M.J., Bizouard, F., Andreux, F., 2006. Emissions and spatial variability of N_2O, N_2 and nitrous oxide mole fraction at the field scale, revealed with ^{15}N isotopic techniques. Soil Biol. Biochem. 38, 941–951. http://dx.doi.org/10.1016/j.soilbio.2005.08.010.

Molodovskaya, M., Warland, J., Richards, B.K., Öberg, G., Steenhuis, T.S., 2011. Nitrous oxide from heterogeneous agricultural landscapes: source contribution analysis by eddy covariance and chambers. Soil Sci. Soc. Am. J. 75, 1829. http://dx.doi.org/10.2136/sssaj2010.0415.

Moore, I.D., Gessler, P., Nielsen, G.A., Peterson, G.A., 1993. Soil attribute prediction using terrain analysis. Soil Sci. Soc. Am. J. 57, 443–452. http://dx.doi.org/10.2136/sssaj1993.572NPb.

Murphy, P.N.C., Ogilvie, J., Arp, P., 2009. Topographic modelling of soil moisture conditions: a comparison and verification of two models. Eur. J. Soil Sci. 60, 94–109. http://dx.doi.org/10.1111/j.1365-2389.2008.01094.x.

Ord, J.K., Getis, A., 2010. Local spatial autocorrelation statistics: distributional issues and an application. Geogr. Anal. 27, 286–306. http://dx.doi.org/10.1111/j.1538-4632.1995.tb00912.x.

Parkin, T.B., 1987. Soil microsites as a source of denitrification variability. Soil Sci. Soc. Am. J. 51, 1194–1199. http://dx.doi.org/10.2136/sssaj1987.03615995005100050019x.

Parkin, T.B., Venterea, R.T., Hargreaves, S.K., 2012. Calculating the detection limits of chamber-based soil greenhouse gas flux measurements. J. Environ. Qual. 41, 705. http://dx.doi.org/10.2134/jeq2011.0394.

Ravishankara, A.R., Daniel, J.S., Portmann, R.W., 2009. Nitrous oxide (N_2O): the dominant ozone-depleting substance emitted in the 21st century. Science 326, 123–125. http://dx.doi.org/10.1126/science.1176985.

Scharf, P.C., Shannon, D.K., Palm, H.L., Sudduth, K.A., Drummond, S.T., Kitchen, N.R., Mueller, L.J., Hubbard, V.C., Oliveira, L.F., 2011. Sensor-based nitrogen applications out-performed producer-chosen rates for corn in on-farm demonstrations. Agron. J. 103, 1683–1691. http://dx.doi.org/10.2134/agronj2011.0164.

Sørensen, R., Seibert, J., 2007. Effects of DEM resolution on the calculation of topographical indices: TWI and its components. J. Hydrol. 347, 79–89. http://dx.doi.org/10.1016/j.jhydrol.2007.09.001.

Sundqvist, E., Persson, A., Kljun, N., Vestin, P., Chasmer, L., Hopkinson, C., Lindroth, A., 2015. Upscaling of methane exchange in a boreal forest using soil chamber measurements and high-resolution LiDAR elevation data. Agric. For. Meteorol. 214-215, 393–401. http://dx.doi.org/10.1016/j.agrformet.2015.09.003.

Turner, P.A., Griffis, T.J., Lee, X., Baker, J.M., Venterea, R.T., Wood, J.D., 2015. Indirect nitrous oxide emissions from streams within the US Corn Belt scale with stream order. Proc. Natl. Acad. Sci. 112, 9839–9843. http://dx.doi.org/10.1073/pnas.1503598112.

Turner, P.A., Baker, J.M., Griffis, T.J., Venterea, R.T., 2016a. The impact of kura clover living mulch on nitrous oxide emissions in a corn/soybean system. J. Environ. Qual. http://dx.doi.org/10.2134/jeq2016.01.0036.

Turner, P.A., Griffis, T.J., Baker, J.M., Lee, X., Crawford, J.T., Loken, L.C., Venterea, R.T., 2016b. Regional-scale controls on dissolved nitrous oxide in the upper Mississippi River. Geophys. Res. Lett. 43, 4400–4407. http://dx.doi.org/10.1002/2013GL058740.

US Department of State, 2014. 2014 United States Climate Action Report.

van den Heuvel, R.N., Hefting, M.M., Tan, N.C.G., Jetten, M.S.M., Verhoeven, J.T.A., 2009. N_2O emission hotspots at different spatial scales and governing factors for small scale hotspots. Sci. Total Environ. 407, 2325–2332. http://dx.doi.org/10.1016/j.scitotenv.2008.11.010.

van den Pol-van Dasselaar, A., Corré, W.J., Priemé, A., Klemedtsson, Å.K., Weslien, P., Klemedtsson, L., Stein, A., Oenema, O., 1998. Spatial variability of methane, nitrous oxide, and carbon dioxide emissions from drained grasslands. Soil Sci. Soc. Am. J. 62, 810–817. http://dx.doi.org/10.2136/sssaj1998.03615995006200030039x.

Vauclin, M., Vieira, S.R., Vachaud, G., Nielsen, D.R., 1983. The use of cokringing with limited field soil observations. Soil Sci. Soc. Am. J. 47, 175–184.

Velthof, G.L., van Groenigen, J.W., Gebauer, G., Pietrzak, S., Jarvis, S.C., Pinto, M., Corré, W., Oenema, O., 2000. Temporal stability of spatial patterns of nitrous oxide fluxes from sloping grassland. J. Environ. Qual. 29, 1397. http://dx.doi.org/10.2134/jeq2000.00472425002900050005x.

Venterea, R.T., 2013. Theoretical comparison of advanced methods for calculating nitrous oxide fluxes using non-steady state chambers. Soil Sci. Soc. Am. J. 77, 709. http://dx.doi.org/10.2136/sssaj2013.01.0010.

Venterea, R.T., Coulter, J.A., 2015. Split application of urea does not decrease and may increase nitrous oxide emissions in rainfed corn. Agron. J. 107, 337. http://dx.doi.org/10.2134/agronj14.0411.

Venterea, R.T., Bijesh, M., Dolan, M.S., 2011. Fertilizer source and tillage effects on yield-scaled nitrous oxide emissions in a corn cropping system. J. Environ. Qual. 40, 1521–1531. http://dx.doi.org/10.2134/jeq2011.0039.

Venterea, R.T., Clough, T.J., Coulter, J.a., Breuillin-Sessoms, F., 2015. Ammonium sorption and ammonia inhibition of nitrite-oxidizing bacteria explain contrasting soil N_2O production. Sci. Rep. 5, 12153. http://dx.doi.org/10.1038/srep12153.

Venterea, R.T., Coulter, J.A., Dolan, M.S., 2016. Evaluation of intensive "4R" strategies for decreasing nitrous oxide emissions and nitrogen surplus in rainfed corn. J. Environ. Qual. http://dx.doi.org/10.2134/jeq2016.01.0024.

Wan, H., Mulla, D.J., Galzki, J.C., 2014. Using LiDAR and geographic information system data to identify optimal sites in southern Minnesota for constructed wetlands to intercept nonpoint source nitrogen. J. Soil Water Conserv. 69, 115A–120A. http://dx.doi.org/10.2489/jswc.69.4.115A.

Weintraub, S.R., Taylor, P.G., Porder, S., Cleveland, C.C., Asner, G.P., Townsend, A.R., 2014. Topographic controls on soil nitrogen availability in a lowland tropical forest. Ecology 96, 1561–1574. http://dx.doi.org/10.1890/14-0834.1.

Yanai, J., Sawamoto, T., Oe, T., Kusa, K., Yamakawa, K., Sakamoto, K., Naganawa, T., Inubushi, K., Hatano, R., Kosaki, T., 2003. Atmospheric pollutants and trace gases factors in an agricultural field. J. Environ. Qual. 32, 1965–1977.

Zhang, W., Montgomery, D.R., 1994. Digital Elevation Model Grid Size, Landscape Representation, and Hyrologic Simulations. 30 pp. 1019–1028.